Optimized two-step growth of large surface two-dimensional boron nitride on Ge (001) films by molecular beam epitaxy

Walter Batista Pessoa, Max Franck, Nicolas Nuns, Jarek Dabrowski, Mohamed Achehboune, Jean-Francois Colomer, Luc Henrard, Mindaugas Lukosius, Xavier Wallart, Dominique Vignaud

▶ **To cite this version:**

Walter Batista Pessoa, Max Franck, Nicolas Nuns, Jarek Dabrowski, Mohamed Achehboune, et al.. Optimized two-step growth of large surface two-dimensional boron nitride on Ge (001) films by molecular beam epitaxy. Applied Surface Science, 2025, 699, pp.163165. 10.1016/j.apsusc.2025.163165 . hal-05039362v2

HAL Id: hal-05039362
https://hal.science/hal-05039362v2

Submitted on 25 Nov 2025

HAL is a multi-disciplinary open access archive for the deposit and dissemination of scientific research documents, whether they are published or not. The documents may come from teaching and research institutions in France or abroad, or from public or private research centers.

L'archive ouverte pluridisciplinaire **HAL**, est destinée au dépôt et à la diffusion de documents scientifiques de niveau recherche, publiés ou non, émanant des établissements d'enseignement et de recherche français ou étrangers, des laboratoires publics ou privés.

Copyright

Optimized two-step growth of large surface two-dimensional boron nitride on Ge (001) films by molecular beam epitaxy

Walter Batista-Pessoa[1], Max Franck[2], Nicolas Nuns[3], Jarek Dabrowski[2], Mohamed Achehboune[4], Jean-Francois Colomer[4], Luc Henrard[4], Mindaugas Lukosius[2], Xavier Wallart[1] and Dominique Vignaud[1]*

[1]University of Lille, CNRS, University Polytechnique Hauts de France, Junia-ISEN, UMR 8520-IEMN F-59000 Lille, France

[2]IHP ó Leibniz-Institut für innovative Mikroelektronik, Im Technologiepark 25, 15236 Frankfurt (Oder), Germany

[3]University of Lille, CNRS, Centrale Lille, University of Artois, IMEC-Institut Michel-Eugène Chevreul F-59000 Lille, France

[4]Laboratoire de Physique du solide, Namur Institute of Structured Matter, University of Namur, Rue de Bruxelles 61, 5000, Namur, Belgium

*corresponding author: dominique.vignaud@univ-lille.fr

keywords:

2D boron nitride

molecular beam epitaxy

step-flow growth

borazine

photoelectron spectroscopy

surface roughness

Abstract

The growth of two-dimensional boron nitride (2D-BN) thin films on Ge (001) has been studied, with the ultimate goal of integrating this material into Si technology. Molecular beam epitaxy was used in a dedicated ultra-high vacuum chamber. To avoid the formation of thermal pits on heating the Ge film above ~760°C, a two-step procedure was optimized. A thin 2D-BN buffer layer is first grown at ~730°C using two independent cells for B and N, aimed at stabilizing the Ge surface and to prevent thermal pits formation upon further heating. The second-step at 800°C makes use of another precursor, gaseous borazine, in the same chamber. The growth proceeds in a step-flow mode, and results in homogeneous nano-crystalline large-surface 2D-BN films with a ~1 nm roughness.

Introduction

Because of its wide bandgap (~6 eV) [1, 2], hexagonal boron nitride (hBN) presents many potential applications as an insulator, such as passivation/tunneling layer in graphene/hBN heterostructures or in combination with transition metal dichalcogenides [3, 4], but also for UV single-photon sources and photonics [5, 6]. Chemical vapor deposition (CVD) is the scalable technique most often used to grow hBN on metallic substrates such as Cu, Ni [7-10], although earlier studies involved molecular beam epitaxy (MBE) [11, 12]. This implies that such hBN film must be separated from the metal substrate before using it in any device, generally by transfer techniques which raise many other problems (e.g. wrinkles, contaminations...) [13, 14]. Growth on non-metallic substrates was also considered, such as sapphire [15-17]. An alternative path would be the direct growth of hBN on materials compatible with Si technology integration. The first obvious choices are Si or SiO_2, onto which nanocrystalline hBN was obtained by CVD [18, 19]. Germanium is however a good alternative for this purpose, as evidenced by the successful growth of graphene on Ge films deposited on Si [20-23]. A few growth studies of hBN on Ge were already published. On the one hand, CVD at pressures above 0.5 Torr was explored with the ammonia-borane NH_3-BH_3 precursor, using a non-standard geometry where the Ge surface is placed face-to-face to a quartz or Si wafer [24-26]. The BN growth generally starts by triangular-shaped domains that eventually coalesce to form an almost complete hBN monolayer. On the other hand, a lower total pressure range (10^{-6} to 10^{-3} Torr) was used with borazine $B_3N_3H_6$ as precursor [27]. Nanocrystalline well-oriented vertically stacked hBN layers were observed at the highest temperature setpoint of 980°C and pressure of 10^{-3} Torr.

It must be remembered that many different polytypes of two-dimensional boron nitride (2D-BN), involving different stacking orders of the same elementary monolayer of BN, are stable with very similar calculated total energies [28, 29]. If hBN is by far the most often cited polytype obtained by CVD, this stacking cannot be taken for granted without experimental verification. Indeed, other stacking such as the rhombohedral rBN (labelled ABC) or the graphite-like Bernal stacking (AB) were observed [29-31]. Because a direct identification of the polytype is complicated [32], we are using the general label 2D-BN for the material described in this article.

We present here an investigation of the growth of 2D-BN on Ge (001) films grown on Si (001) in a MBE chamber, in the lowest pressure range (up to 10^{-5} Torr) compared to previously published studies [24-27]. This choice of substrate and orientation was imposed by

the goal of Si technology integration. We took advantage of an uncommon combination of sources in the same chamber, involving a high temperature B cell, a N_2 RF plasma cell and a gaseous borazine injector. The growth conditions were optimized, which led to a two-step process. A buffer layer is first grown at ~730°C using independent B and N cells, to stabilize the surface. The main 2D-BN layer is then grown at 800°C under borazine flow which results in a step-flow growth of multilayer 2D-BN.

1. Experiments

All growth experiments used 2 μm thick epitaxial Ge (001) films deposited by CVD on Si (001) substrate [33], sawn into 1x1 cm² pieces. 2D-BN films were grown by MBE in a commercial Riber ultra-high vacuum (UHV) chamber. An infrared pyrometer at 0.85 μm wavelength was used for growth temperature measurements above 700°C (uncorrected for emissivity, corresponding to 730°C after correction). This induces a larger uncertainty on the temperature of samples grown at 730°C than to higher ones, which justifies to write ~730°C only in this specific case. More details about this chamber were already published [34-36]. Two independent configurations of precursors were used to grow 2D-BN. The first one involved separated cells for B and N, that is a high-temperature effusion cell for boron (HTEZ from MBE-Komponenten) combined with a nitrogen radio-frequency valved plasma cell (VRF-N-600 from Riber) [36]. Under these conditions, the chamber pressure is ~10^{-5} Torr, depending on the N_2 flow (5 sccm). The second precursor is gaseous borazine ($B_3N_3H_6$), providing both B and N atoms, entering the growth chamber through a Mo gas injector which may be heated to temperatures up to 1100°C [34]. The borazine pressure is regulated before entering the injector through a calibrated hole. A set-point of 5 Torr corresponds to an equilibrium pressure of ~3.10^{-6} Torr in the MBE chamber.

Once grown, samples were transferred after a short air exposure in a separated X-ray photoelectron spectroscopy (XPS) chamber for chemical analysis (stoichiometry) as well as for a 2D-BN thickness estimation. A Physical Electronics 5600 spectrometer fitted in an UHV chamber (base pressure ~$1\cdot10^{-10}$ Torr) was used, with a monochromatized Al anode X-ray source (photon energy 1487 eV) and a typical probe size of 400 μm diameter. A gold reference sample was measured and the position of the Au 4f 7/2 photoemission peak at 84.0 eV [37] was used to calibrate the binding energy scale. The B/N composition ratio was determined from the I_{B1s}/I_{N1s} ratio [35], after correction for the respective sensitivities of the

set-up. I_{B1s} (respectively I_{N1s}) represents the integrated intensity of the BN-related B 1s (N 1s) component after background subtraction according to the Shirley procedure [38]. The ratios I_{B1s}/I_{Ge} and I_{N1s}/I_{Ge} obtained for different photoelectron angles were used to estimate the ratio $d/\lambda_{B,BN}$ based on a homogeneous thickness single layer model [34, 35]. $\lambda_{B,BN}$ is the inelastic mean free path of B photoelectrons in BN, and d is the averaged BN thickness. I_{Ge} stands for the integrated intensity of the Ge film peak, using either the Ge3s or Ge3d components which led to very similar estimates. The photoelectron takeoff angle was varied between 25° (close to grazing incidence, surface sensitive) and 75° (nearly normal incidence, bulk sensitive). Atomic Force Microscopy (AFM) observations and roughness measurements were achieved in air in tapping mode using a Multimode Veeco equipment with a Nanoscope IVa controller. All the roughness values reported here were obtained on 1x1 µm² surfaces. Time-of-flight Secondary Ion Mass Spectroscopy (ToF-SIMS) measurements were realized with a TOF SIMS.5 system (IONTOF). The burst (respectively bunch) mode was used for mapping (spectroscopy), using 25 keV Bi^+ as primary ion source. The BN content was studied by measuring the ^{10}BN signal. The typical spatial resolution is 200 nm for mapping. X-ray reflectivity (XRR) experiments were carried out using a Rigaku SmartLab diffractometer with a 9 kW Cu-Kα rotating anode, at a wavelength of 1.5418 Å. The beam size projected on the sample surface, which depends on the incidence angle, is always larger than 10 mm² for the considered incidence angle range. High-resolution transmission electron microscopy (HRTEM) images were acquired using a FEI Tecnai Osiris microscope operated at 200 kV. This microscope features a Schottky field emission gun and offers a lateral resolution of 0.26 nm in HRTEM mode. A Horiba Scientific LabRAM HR confocal spectrometer with a 473 nm laser (power ~10mW) was used for Raman spectroscopy. The beam was focused to a size smaller than 1 µm by a 100x objective.

2. Results and discussion

The choice of the growth temperature is often critical whatever the particular technique, and depends on many parameters. In the case of MBE, a general rule states that the higher the temperature, the higher the adatom mobility and the film crystallographic quality, as long as the film does not start to degrade because of atom sublimation and/or diffusion into the substrate. In the case of the 2 µm Ge film on Si, the optical microscopy images of the surface are shown as a function of the anneal temperature in Fig.1. The Ge surface is strongly

degraded at 850°C and above. For lower temperatures, square thermal pits are observed between 760°C and 820°C. Their size (up to 7 µm edge length) and density ($5x10^4$ to $5x10^5$ pits/cm²) increase with the temperature. Such pits were already described in the literature, with very similar characteristics (onset of appearance at ~750°C, densities in the 10^5 pits/cm² range) [39, 40]. They were associated in bulk Ge either with the desorption from strained regions around dislocation pile-ups [39] or with the preferential evaporation of Ge suboxides [40]. We tried to etch these suboxides, thanks to a HBr-based process [40], but it showed a rather limited efficiency on annealing with our samples (reduction of the pit density from ~1.8 10^5 down to ~1.3 10^5 pits/cm²). So, the highest temperature that may be used without surface degradation because of thermal pit appearance is ~730°C, which is thus the maximum usable temperature for direct growth of 2D-BN on Ge films.

2.1 One-step growth, choice of B source

Given the temperature restriction previously described, the growth of 2D-BN was explored using either borazine or the combination of boron evaporation and nitrogen plasma cells. The B 1s and N 1s XPS spectra of these samples are summarized in Fig.2, while the corresponding growth parameters are detailed in Table 1. These initial sets were selected according to previous experiments on Ni [34-36]. All spectra show one single peak at ~398.4 eV in the N 1s range corresponding to B-N bonds. In the B 1s spectral domain, a main peak at ~190.7 eV is always observed, associated with B-N bonds. For all samples except A600 which is B-rich (B/N~1.4), the B/N atomic ratio is 1±0.1 (see Table 1), that is the stoichiometry expected for 2D-BN, when one considers only the BN-related peaks at ~190.7 eV and ~398.4 eV. Some samples also show an additional component at ~188 eV, most probably related to parasitic B-B bonds [41-43]. This last observation implies that the corresponding 2D-BN films are B-rich, and should thus be avoided. In the case of the borazine precursor (the Axxx set of samples), there is no direct way of adjusting independently the B and N flow since a single (stoichiometric) precursor is used. Both samples A600 and A730 show a significant B-B component relative to the B-N one, so borazine does not appear to be a good choice of precursor to grow 2D-BN directly on Ge.

Considering now the set of samples grown from separated B and plasma-activated N_2 (the Bxxxx samples), the only one for which a strong 188 eV peak is detected was grown with the highest B-cell temperature (1800°C), that is the highest B flux. Reducing the B-cell temperature to 1720 or 1760°C (and thus the B flux) is sufficient to avoid the formation of the unwanted B-B bonds. The B/N composition remains slightly B-rich at 1760°C, with a B/N

composition ratio of 1.07, and is closer to ideal stoichiometry at 1720°C (B/N~0.96). A B-cell temperature of 1720°C was systematically used in the following studies.

2.2 One-step growth, characterization

The growth temperature being set at ~730°C, we have studied how the thickness and surface morphology of the 2D-BN grown on Ge depends on the growth duration. This is illustrated in Fig. 3, where the surface rms roughness measured by AFM (Fig. 3a) and the normalized 2D-BN thickness estimated from XPS intensity ratios (Fig.3b) are plotted (see grey triangle curves). AFM topographic images are presented in the supplementary material figure S1. It shows that the rms roughness and the thickness increase almost linearly with time. Using a calculated value for the inelastic mean free path of 3.3 nm [44], one obtains a growth rate of ~4 monolayers/h (ML/h) and a roughness increase rate of ~0.5 nm/h (equivalent to ~1.5 ML/h). This surface roughness is illustrated in Fig. 4a by a HRTEM cross-section of a 2D-BN sample grown for 1 hour at ~730°C. As can be seen, the Ge substrate remains almost atomically flat at this temperature, and the increased surface roughness is entirely due to the 2D-BN overlayer. The average thickness determined by XPS for this sample is ~5 ML and the roughness is ~1 nm (including the initial Ge film rms roughness of 0.4 nm), which is corroborated by the HRTEM cross-section. The 2D-BN grain size is relatively small (in the nm range), which can be attributed to the low growth temperature necessary to avoid the formation of thermal pits. These results, and particularly the roughness increase rate with BN thickness, implies that using such 2D-BN would be restricted only to very simple applications in the case of 2D heterostructures. We assume that the bottleneck is the limitation on the growth temperature to avoid the formation of thermal pits. The adatom mobility on the surface is then too low, which results in the large increase of the roughness with the 2D-BN thickness.

A few samples were analysed by ToF-SIMS after being stored for a few weeks in air. The corresponding maps for the $^{10}BN^-$ and GeO_2^- signals are shown in Fig. 5, measured on samples grown for 2, 10 and 60 min. The homogeneous spatial distribution of the BN film is evident (Fig. 5a, c and e). The main difference lies in the GeO_2^- maps (Fig. 5 b, d and f). While the Ge substrate is still clearly oxidized after 2 min, no trace of GeO_2 could be found after 10 min or 60 min growth (see also Fig. 5g). This reduction of the GeO_2^- signal coincides with the appearance of a BO^- component (see Fig 5g), induced by the long air exposure of the

2D-BN since it was not detected by XPS immediately after growth. This suggests that the 10 min BN film completely covers the surface and prevents the Ge oxidation during air exposure. Next, we have studied the surface stability of a thin 2D-BN buffer layer grown at ~730°C on a Ge film during post-growth annealing up to 850°C. It turns out that thermal pits do not appear as long as the post-growth anneal temperature does not exceed 810°C. For higher temperatures, the surface is destroyed, similarly to what was obtained without the 2D-BN buffer layer (see Fig. 1, 850°C case). The surface stability on annealing did not appear to depend on the 2D-BN thickness, a 10 min buffer layer being sufficient to avoid thermal pit formation. In some limited cases, a few thermal pits were found but at much lower densities (Ö 10^3 pits/cm^2) than previously observed without the buffer layer. Such buffer layer could be used to protect the surface at temperatures higher than ~730°C, thus allowing to study the 2D-BN growth in an extended temperature range.

2.3 Two-step growth

Based on the previously described set of results, a two-step process was developed, involving the growth of an initial 2D-BN buffer layer for 10 min at ~730°C, followed by a second high-temperature step at 800°C for a variable duration. We started by using the same precursors for both steps, that is the B high-temperature cell and the N plasma cell. Once the growth of the buffer layer was completed, the temperature was raised over a few minutes to 800°C without atomic flux interruption. Thermal pits were not observed, confirming the efficiency of the buffer layer to prevent the degradation of the surface. The corresponding XPS spectra (not shown) are similar to the ones obtained for the samples B1720 or B1760 (see Fig. 2), without any B-B component at ~188 eV and with the expected B/N composition ratio B/N = 1±0.1. The surface roughness and the total thickness again increase almost linearly with growth time (see Fig. 3, blue curves and squares), although both curves present slopes approximately reduced by a factor of ~2 compared to the growth at ~730°C (growth rate ~2 ML/h and roughness increase ~0.25 nm/h). So, the roughness vs thickness curve is similar to what is obtained with the one-step growth at ~730°C, making the two-step procedure unable to improve the 2D-BN quality with this set of precursors. The growth rate reduction might be understood by the onset of some sublimation mechanism that would start to become efficient at ~800°C when using independent B and N precursors. Preliminary ab initio density functional theory (DFT) simulations suggests that desorption at the atomic level could not explain a two-times reduction of the growth rate. One may thus speculate that larger

clusters could be involved, such as full BN ring that would desorb much more efficiently at 800°C than at 730°C.

The borazine could not be used as a precursor for the 2D-BN buffer growth on Ge at ~730°C because of the observation of unwanted B-B bonding (see section 2.1). Because of the potentially favourable temperature evolution of the B/N atomic ratio using borazine (compare the stoichiometry between samples A600 and A730, see Table 1), we have also explored a modified two-step process with a different set of precursors for each step. After the growth of the buffer layer at ~730°C (step 1), the temperature was raised to 800°C over a few minutes without any atomic flux, and the growth was then started using borazine (step 2). The XPS spectra (not shown) obtained with the two-step process using borazine as the only precursor during step 2 are identical to the ones measured on the B1720 sample. They do not show any ~188 eV parasitic component, contrary to what was observed at lower temperature (see Fig. 2). The ratio of the XPS integrated intensities led to a composition ratio B/N = 1±0.05, indicating the expected stoichiometry for 2D-BN. Thermal pits were again not detected. The thickness and roughness time dependency are shown in Fig. 3 (red curves and squares). From this curve, it appears that the growth rate increased to ~5 ML/h. More interesting, the roughness tends to saturate with time and/or thickness to a value of ~1.0 nm: contrary to what is occurring in the case of independent B and N precursors, there is almost no increase of the roughness when borazine is used for the second step. So, we now call this process the optimized two-step process. The thickness-independent roughness might be understood on the basis of DFT simulations [27]. When borazine is the precursor, it was calculated that growth only occurs at the edges of the 2D-BN film in a step-flow mode, because borazine molecules desorb very rapidly from a perfect 2D-BN surface. Because the roughness continuously increases when independent cells are used for B and N, one may speculate that the 2D-BN film growth no longer proceeds in this case by step-flow, but rather by some 3D island nucleation mode.

The improvement of the 2D-BN quality clearly appears on the HRTEM cross-section presented in Fig. 4b. Note that the Ge interface did not roughen despite the increased temperature, due to being protected by the buffer layer. The thickness of the 2D-BN film is increased to ~9 ML, consistent with the XPS measurements, while the surface roughness is slightly reduced compared to Fig. 4a, to 0.8 nm according to the AFM measurements. While the grain size remains small, in the few nm range, the homogeneity of the film thickness is much better thanks to the optimized two-step growth process. This is confirmed by the XRR

curves presented in Fig. 6. All samples prepared using the optimized procedure show clear X-ray reflectance oscillations, from which one may deduce the layer thickness and roughness from the best fit of these experiments (using the Smartlab Studio II software). The observation of these oscillations shows the uniformity of the XRR thickness and roughness over the whole probed area. The black curve in Fig. 6 shows the XRR measurement obtained on a sample grown by the two-step process with the same set of precursors (independent B and N cells) used for both steps. A unique satisfying fit cannot be obtained, because of the too large thickness fluctuations, so we could only determine the roughness by setting the thickness as estimated from the XPS measurement. If one compares the XRR curves drawn in red and black, corresponding to similar average thicknesses as determined by XPS (see table 2), the XRR oscillations are only observed when borazine is used for the second step growth, which emphasizes the large-scale thickness uniformity in this case. The XRR-determined thickness and roughness measurements are gathered in Table 2, together with the ones obtained by independent techniques such as XPS or HRTEM (for the thickness) and AFM (roughness). There is a clear consistency between all measurements, despite the very different probe size, from a few nm (HRTEM) to a few mm (XRR). This coherence between independent measurements emphasizes the large-scale homogeneity of the 2D-BN thickness obtained using the two-step optimized process. The samples grown by the optimized process were finally studied by Raman spectroscopy (see Fig. 7). The 2D-BN E_{2g} peak was observed for the thickest samples ($\times$ 20 ML, corresponding to 4 h or more growth duration) at 1372 ± 2 cm^{-1}, with a typical full width at half maximum of ~40 cm^{-1}. The weak intensities and the large peak width probably come from the limited size of the 2D-BN grains, as shown by HRTEM in Fig. 4b.

Conclusion

In this work, we have studied the 2D-BN growth process on Ge (001) films by MBE. Because of the temperature limitation set by the formation of thermal pits, a two-step optimized process was developed, involving the growth of a thin 2D-BN buffer layer at ~730°C using independent B and N cells, followed by an 800°C second growth step using borazine. The 2D-BN growth rate is ~5 ML/h, with a roughness of ~1 nm independent of thickness. The thin 2D-BN buffer layer (~1 ML thick) prevents the nucleation of thermal pits during the high temperature step. Although the grain size remains low, in the few nm range, the 2D-BN thickness is homogeneous on a large surface at the wafer scale.

Acknowledgments: The work was funded by the 2DHetero FLAG-ERA 2019 project. IEMN acknowledges the French RENATECH network for its financial support, and the Chevreul Institute (CNRS FR2638) for funding the X-ray facilities. IHP was funded by the Deutsche Forschungsgemeinschaft (DFG, 436545422). IHP acknowledges the Gauss Centre for Supercomputing e.V. (www.gauss-centre.eu) for funding this project by providing computing time through the John von Neumann Institute for Computing (NIC) on the GCS Supercomputer JUWELS at Jülich Supercomputing Centre (JSC). University of Namur thanks the support of the Fonds de la Recherche Scientifique (F.R.S.-FNRS, project R.8009.19). We would also like to thank Dr. Markus Andreas Schubert (IHP) for the HRTEM characterization and Christophe Boyaval (IEMN) for assitance with SEM analysis.

Biblio

[1] Watanabe K., Taniguchi T., Niiyama T., Miya K., Taniguchi M., Far-ultraviolet plane-emission handheld device based on hexagonal boron nitride, Nature Photonics 3, 591 (2009) doi: 10.1038/nphoton.2009.167

[2] Sponza L., Amara H., Attaccalite C., Latil S., Galvani T., Paleari F., Wirtz L., Ducastelle F., Direct and indirect excitons in boron nitride polymorphs: A story of atomic configuration and electronic correlation, Phys. Rev. B 98, 125206 (2018) doi: 10.1103/PhysRevB.98.125206

[3] Zhang J., Tan B., Zhang X., Gao F., Hu Y., Wang L., Duan X., Yang Z., Hu P, Atomically thin hexagonal boron nitride and its heterostructures, Adv. Mater. 33, 2000769 (2021) doi: 10.1002/adma.202000769

[4] Lin Y.C., Torsi R., Younas R., Hinkle C.L., Rigosi A.F. et al., Recent advances in 2D material theory, synthesis, properties, and applications ACS Nano 17, 9694 (2023) doi: 10.1021/acsnano.2c12759

[5] Caldwell J.D., Aharonovich I., Cassabois G., Edgar J.H., Gil B., Basov D.N., Photonics with hexagonal boron nitride, Nature Mater. 4, 552 (2019) doi: 10.1038/s41578-019-0124-1

[6] Michaelis de Vasconcellos S., Wigger D., Wurstbauer U., Holleitner A.W., Bratschitsch R., Kuhn T., Single photon emitters in layered Van der Waals materials, Phys. Stat. Sol. B 259, 2100566 (2022) doi: 10.1002/pssb.202100566

[7] Song L., Ci L., Lu H., Sorokin P.B., Jin C., Ni J., Kvashnin A.G., Kvashnin D.G., Lou J., Yakobson B.I., Ajayan P.M., Large scale growth and characterization of atomic hexagonal boron nitride layers, Nano Lett. 10, 3209 (2010) doi: 10.1021/nl1022139

[8] Shi Y., Hamsen C., Jia X., Kim K.K., Reina A. et al., Synthesis of few-layer hexagonal boron nitride thin film by chemical vapor deposition, Nano Lett. 10, 4134 (2010) doi: 10.1021/nl1023707

[9] Li L., Zhang R., Zhang R., Han Z., Dong H., Yu G., Geng D., Yang H.Y., A minireview on chemical vapor deposition growth of wafer-scale monolayer h-BN single crystals, Nanoscale 13, 17310 (2021) doi: 10.1039/d1nr04034k

[10] Naclerio A.E., Kidambi P.R., A review of scalable hexagonal boron nitride (h-BN) synthesis for present and future applications, Adv. Mater. 35, 2207374 (2023) doi: 10.1002/adma.202207374

[11] Nagashima A., Tejima N., Gamou Y., Kawai T., Oshima C., Electronic dispersion relations of monolayer hexagonal boron nitride formed on the Ni(111) surface, Phys. Rev. B 51, 4606 (1995) doi: 10.1103/PhysRevB.51.4606

[12] Auwärter W., Kreutz T.J., Greber T., Osterwalder J., XPD and STM investigation of hexagonal boron nitride, Surf. Sci. 429, 229 (1999) doi: 10.1016/S0039-6028(99)00381-7

[13] Li X., Zhu Y., Cai W., Borysiak M., Han B., Chen D., Piner R.D., Colombo L., Ruoff R.S. Transfer of large-area graphene films for high-performance transparent conductive electrodes, Nano Lett 9, 4359 (2009) doi: 10.1021/nl902623y

[14] Lupina G., Kitzmann J., Costina I., Lukosius M., Wenger C. et al., Residual metallic contamination of transferred chemical vapor deposited graphene, ACS Nano 9, 4776 (2015) doi: 10.1021/acsnano.5b01261

[15] Kobayashi Y., Akasaka T., Hexagonal BN epitaxial growth on (0001) sapphire substrate by MOVPE, J. Crystal Growth 310, 5044 (2008) doi: 10.1016/j.jcrysgro.2008.07.010

[16] Jang A.R., Hong S., Hyun C., Yoon S.I., Kim G. et al., Wafer-scale and wrinkle-free epitaxial growth of single-orientated multilayer hexagonal boron nitride on sapphire, Nano Lett. 16, 3360 (2016) doi: 10.1021/acs.nanolett.6b01051

[17] Vuong T.Q.P., Cassabois G., Valvin P., Rousseau E., Summerfield A. et al., Deep ultraviolet emission in hexagonal boron nitride grown by high-temperature molecular beam epitaxy 2D, Mater. 4, 021023 (2017) doi: 10.1088/2053-1583/aa604a

[18] Tay R.Y., Tsang S.H., Loeblein M., Chow W.L., Loh G.C;, Toh J.W., Ang S.L., Teo E.H.T. Direct growth of nanocrystalline hexagonal boron nitride films on dielectric substrates, Appl. Phys. Lett. 106, 101901 (2015) doi: 10.1063/1.4914474

[19] Behura S., Nguyen P., Debbarma R., Che S., Seacrist M.R., Berry V., Chemical interaction-guided, metal-free growth of large-area hexagonal boron nitride on silicon-based substrates, ACS Nano 11, 4985 (2017) doi: 10.1021/acsnano.7b01666

[20] Wang G., Zhang M., Zhu Y., Ding G., Jiang D., Guo Q., Liu S., Xie, X., Chu P. K., Di Z., Wang X., Direct growth of graphene film on germanium substrate, Sci. Rep. 3, 2465 (2013) doi: 10.1038/srep02465

[21] Lee J.H., Lee E.K., Joo W.J., Jang Y., Kim B.S. et al., Wafer-scale growth of single-crystal monolayer graphene on reusable hydrogen-terminated germanium, Science 344, 286 (2014) doi: 10.1126/science.1252268

[22] Lukosius M., Dabrowski J., Kitzmann J., Fursenko O., Akhtar F. et al., Metal-free CVD graphene synthesis on 200 mm Ge/Si(001) substrates, ACS Appl. Mater. Interfaces 8, 33786 (2016) doi: 10.1021/acsami.6b11397

[23] Lee J.H., Kang S.G., Jang H.S., Moon J.Y., Whang D., Graphene on group-IV elementary semiconductors: the direct growth approach and its applications, Adv. Mater. 31, 1803469 (2019) doi: 10.1002/adma.201803469

[24] Yin J., Liu X., Lu W., Li J., Cao Y., Li Y., Xu Y., Li X., Zhou J., Jin C., Guo W., Aligned growth of hexagonal boron nitride monolayer on germanium, Small 11, 5375 (2015) doi: 10.1002/smll.201501439

[25] Hong M.K., Hyun S.H., Jang H.S., An B.S., Jang H.C. et al., Controlled growth of in-plane graphene/h-BN heterostructure on a single crystal Ge substrate, App. Surf. Sci. 554, 149655 (2021) doi: 10.1016/j.apsusc.2021.149655

[26] Zhang C., Gao B., Ran Y., Shi Z., Zhu H., Zhang H., Liu J., Yang B., Liu Z., Wu T., Xie X., Silicon-assisted growth of hexagonal boron nitride to improve oxidation resistance of germanium, 2D Mater. 8, 035041 (2021) doi: 10.1088/2053-1583/ac0298

[27] Franck M., Dabrowski J., Schubert M.A., Wenger C., Lukosius M., Towards the growth of hexagonal boron nitride on Ge(001)/Si substrates by chemical vapor deposition, Nanomaterials 12, 3260 (2022) doi: 10.3390/nano12193260

[28] Constantinescu G., Kuc A., Heine T., Stacking in bulk and bilayer hexagonal boron nitride, Phys. Rev. Lett. 111, 036104 (2013) doi: 10.1103/PhysRevLett.111.036104

[29] Gilbert SM, Pham T., Dogan M., Oh S., Shevitski B., Schumm G., Liu S., Ercius P., Aloni S., Cohen M.L., Zettl A., Alternative stacking sequences in hexagonal boron nitride, 2D Mater. 6, 021006 (2019) doi: 10.1088/2053-1583/ab0e24

[30] Chubarov M., Pedersen H., Högberg H., Darakchieva V., Jensen S., Persson P.O.A., Henry A., Epitaxial CVD growth of sp^2-hybridized boron nitride using aluminum nitride as buffer layer, Phys. Status Solidi RRL 5, 397 (2015) doi: 10.1002/pssr.201105410

[31] Prevost H., Andrieux-Ledier A., Dorval N., Fossard F., Mérot J.S., Schué L., Plaud A., Héripré E., Barjon J., Loiseau A., Heteroepitaxial growth of sp^2-hybridized boron nitride multilayer on nickel substrates by CVD: the key role of the substrate orientation, 2D Mater. 7, 045018 (2020) doi: 10.1088/2053-1583/aba8ad

[32] Zanfrognini M., Plaud A., Stenger I., Fossard F., Sponza L. et al., Distinguishing different stackings in layered materials via luminescence spectroscopy, Phys. Rev. Lett. 131, 206902 (2023) doi: 10.1103/PhysRevLett.131.206902

[33] Yamamoto Y., Zaumseil P., Arguirov T., Kittler M., Tillack B., Low threading dislocation density Ge deposited on Si (100) using RPCVD, Solid-State Electronics 60, 2 (2011) doi: 10.1016/j.sse.2011.01.032

[34] Hadid J., Colambo I., Boyaval C., Nuns N., Dudin P., Avila J., Wallart X., Vignaud D., Molecular beam epitaxial growth of hexagonal boron nitride on Ni foils, 2D Mater. 8, 045007 (2021) doi: 10.1088/2053-1583/ac1502

[35] Hadid J., Colambo I., Avila J., Plaud A., Boyaval C. et al., Molecular beam epitaxial growth of multi-layer 2D-boron nitride on Ni substrates from borazine and plasma-activated nitrogen, Nanotech. 34, 035601 (2023) doi: 10.1088/1361-6528/ac99e5

[36] Batista-Pessoa W., Wallart X., Vignaud D., Two dimensional boron nitride growth on nickel foils by plasma assisted molecular beam epitaxy from elemental B and N sources, Nanotech. 34, 415601 (2023) doi: 10.1088/1361-6528/ace450

[37] Moulder J.F., Stickle W.F., Sobol P.E., Bomben K. D. and Chastain J., Handbook of X-Ray Photoelectron Spectroscopy, Perkin-Elmer, Eden Prairie, MN, 1992

[38] Shirley D.A., High-resolution X-Ray photoemission spectrum of the valence bands of gold, Phys. Rev. B 5, 4709 (1972) doi: 10.1103/PhysRevB.5.4709

[39] Persichetti L., Fanfoni M., De Seta M., Di Gaspare L., Ottaviano L., Goletti C., Sgarlata A., Formation of extended thermal etch pits on annealed Ge wafers, Appl. Surf. Sci. 462, 86 (2018) doi: 10.1016/j.apsusc.2018.08.075

[40] Diallo T.M., Aziziyan M.R., Arvinte R., Arès R., Fafard S., Boucherif A., CVD growth of high-quality graphene over Ge (100) by annihilation of thermal pits, Carbon 174, 214 (2021) doi: 10.1016/j.carbon.2020.12.024

[41] Li H., Li H., Dai W.L., Wang W., Fang Z., Deng J-D, XPS studies on surface electronic characteristics of Ni-B and Ni-P amorphous alloy and its correlation to their catalytic properties, Appl. Surf. Sci. 152, 25 (1999) doi: 10.1016/S0169-4332(99)00294-9

[42] Kidambi P.R., Blume R., Kling J., Wagner J. B., Baehtz C., Weatherup R. S., Schloeg R., Bayer B.C. & Hofmann S., In situ observations during chemical vapor deposition of hexagonal boron nitride on polycrystalline copper, Chem. Mater. 26, 6380 (2014) doi: 10.1021/cm502603n

[43] Feng B., Zhang J., Zhong Q., Li W., Li S., Li H., Cheng P., Meng S., Chen L., Wu K., Experimental realization of two-dimensional boron sheets, Nat. Chem. 8, 563 (2016) doi: 10.1038/NCHEM.2491

[44] Powell C J et al (2011) NIST electron effective attenuation-length database, version 1.3, standard reference data program database 82 (Gaithersburg, MD: National Institute of Standards and Technology) (available at: www.nist.gov/srd/nist-standard-reference-database-82)

Tables:

sample	T (°C)	A- borazine pressure - injector temperature B- N_2 flow - RF power - B temperature	duration (min)	B/N
A600	~600	5 Torr - 300°C	60	1.4
A730	~730	5 Torr - 300°C	60	1.01
B1800	~730	5 sccm - 580 W - 1800°C	60	1.08
B1760	~730	5 sccm - 580 W - 1760°C	60	1.07
B1720	~730	5 sccm - 580 W - 1720°C	60	0.96

Table 1: initial set of growth parameters (growth temperature, precursor cell settings and growth duration). B/N is the atomic composition ratio measured by XPS. Samples with a label starting by A (respectively B) were grown from borazine (separated B and N_2 plasma). The number following the initial capital letter corresponds to the growth temperature for set A and to the B cell temperature in case B.

growth (h)	thickness (nm)			rms roughness (nm)	
	XPS	XRR	HRTEM	XRR	AFM
1	1.7	2.0		1.0	0.7
2	3.5	2.8	2.3 - 3.8	1.1	0.8
4	7.3	6.2		1.3	1.0
4 (B+N)*	3.6			2.8	1.5

Table 2: thickness, independently determined by XPS, XRR and HRTEM, and surface roughness from XRR and AFM, for samples grown with the optimized two-step BN growth on Ge for 1h, 2h and 4h. * Sample grown using the same precursors (separated B and N cells) for both steps. Because no oscillations could be observed on the reflectometry curve, the XRR roughness was estimated by fixing the thickness as determined from the XPS data.

Figures:

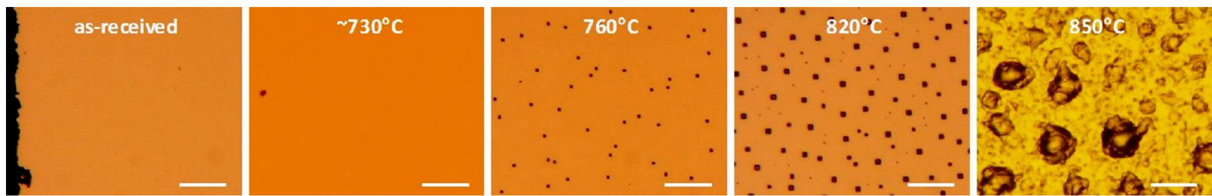

Fig. 1: optical microscopy images (10x objective) of the Ge (001) surface as a function of the anneal temperature (all scale bars are 50 µm).

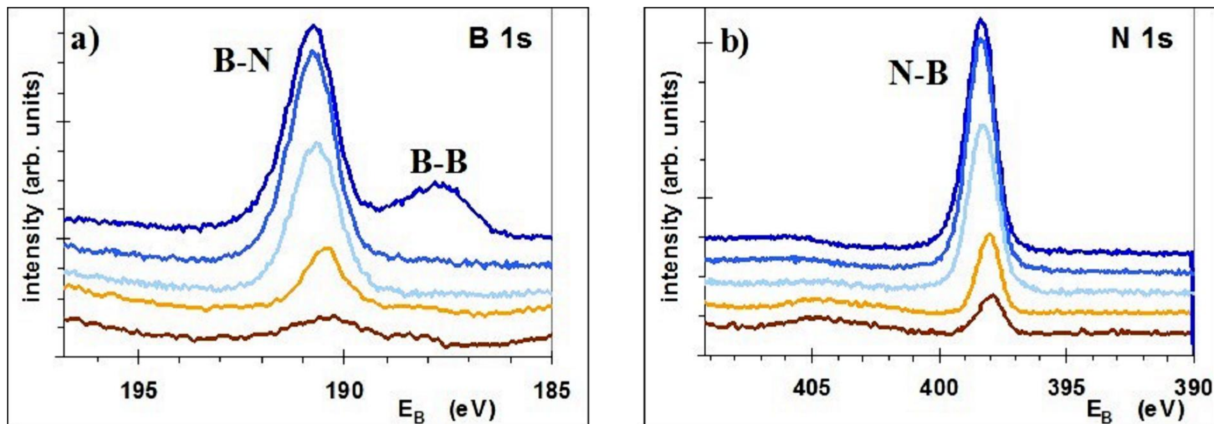

Fig. 2: XPS core level spectra for B 1s (a) and N 1s (b) after 2D-BN growth on Ge for 1 h. From bottom to top, samples are A600, A730, B1720, B1760 & B1800 (details in Table 1). The intensity for the A-sample spectra were corrected for a 25% decrease of the anode emissivity compared to the other samples (spectra are vertically shifted for clarity).

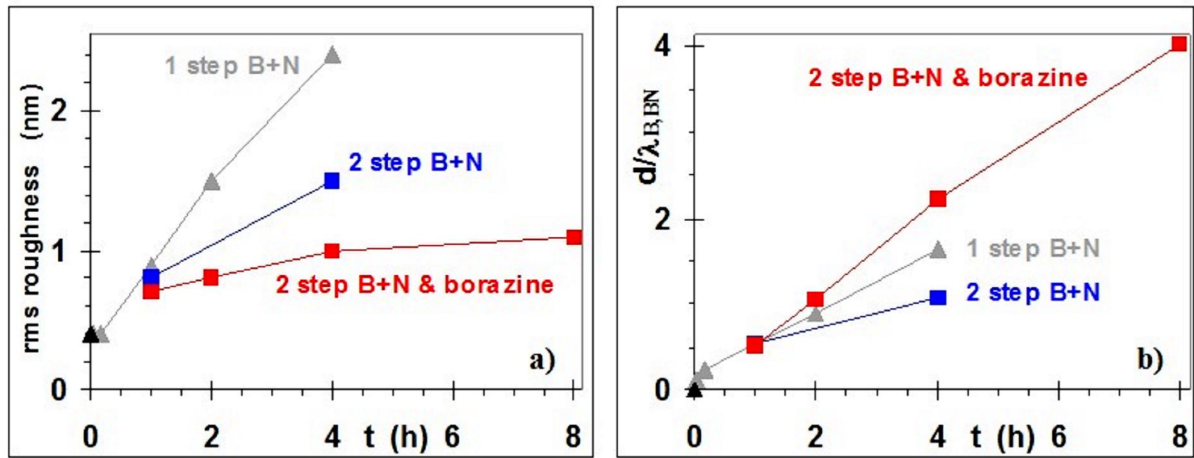

Fig. 3: a) surface rms roughness as measured by AFM on 1x1 µm² area and b) normalized 2D-BN thickness $d/\lambda_{B,BN}$ estimated from XPS integrated intensity ratios, vs the total growth time. The grey triangles are for one-step growth at ~730°C, squares for two-step growth at ~730°C and 800°C. The 2nd step precursors are B and activated N (blue squares) or borazine (red squares). The black triangle is for a reference Ge (001) film on Si without 2D-BN. Lines are just guides.

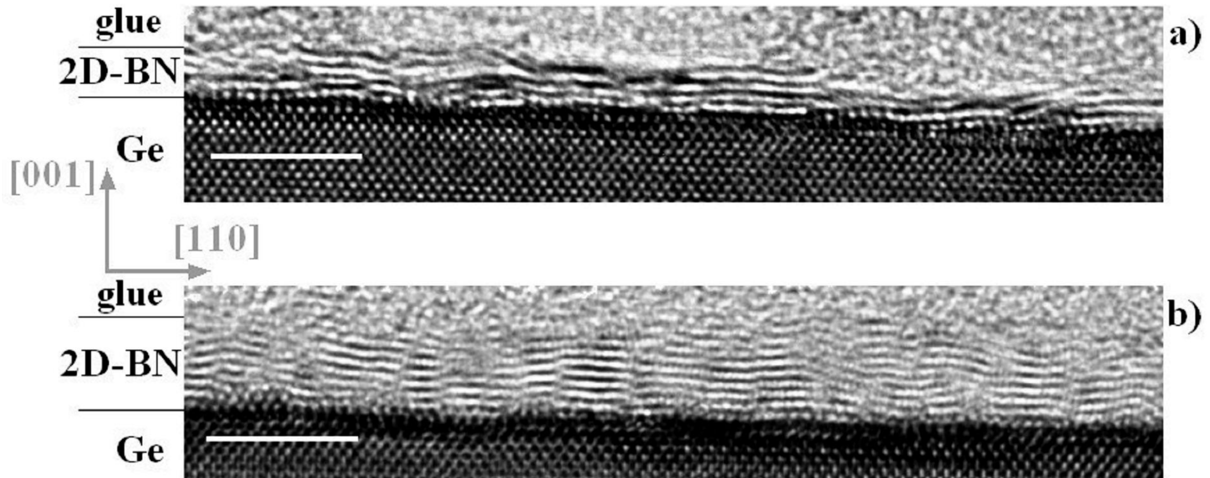

Fig. 4: HRTEM cross-section images of 2D-BN grown on a Ge (001) film, a) one-step at ~730°C (60 min), and b) two-steps at ~730°C (10 min) and 800°C (120 min). The glue used for HRTEM sample preparation appears above the 2D-BN layer. Scale bars are 5 nm.

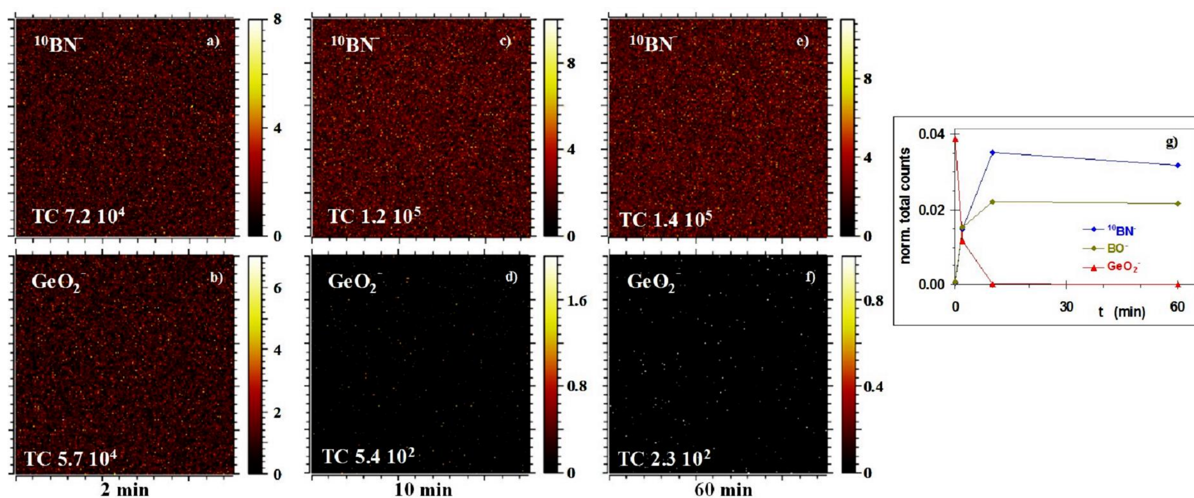

Fig. 5: ToF-SIMS analysis of the $^{10}BN^-$ (a, c, e) and of the GeO_2^- (b, d, f) spatial counts on 100x100 µm² area, after 2 min (a, b), 10 min (c, d) and 60 min (e, f) growth at ~730°C, where TC stands for the corresponding total map count, g) total count evolution of selected components vs growth time, normalized to the total ion intensity (lines are just guides).

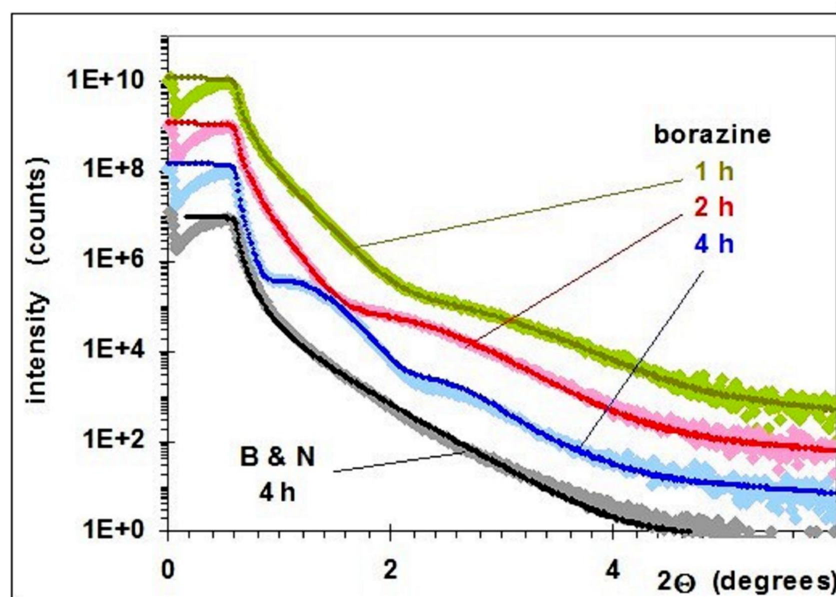

Fig. 6: X-ray reflectivity curves for 2D-BN samples grown using borazine during the 2nd step, for 1 h (green), 2 h (red) and 4 h (blue), from top to bottom. The corresponding fits are superposed in darker color. The bottom black line comes from a sample grown using independent B and N cells for 4 h. The large roughness prevents a useful fit in this case. Spectra are vertically shifted for clarity.

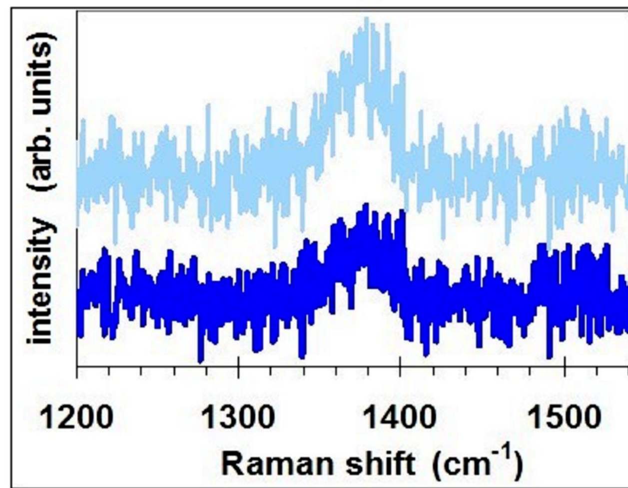

Fig. 7: Raman spectra of 2D-BN samples grown using the optimized process on Ge (001) films for 4 h (dark blue) and 8 h (light blue). Spectra were vertically shifted for clarity.